Nano Research

Open Access

Research Article

Biocompatible copper single-atom site nanozyme for parallel tumor therapy

Haining Zhou[1,§], Hui Peng[5,§], Yugui Lian[3], Ting Sun[4] ✉, Chang Su[2] ✉, and Zhiyuan Wang[6]

[1] *Department of Gastroenterology, the First Affiliated Hospital of Zhengzhou University, Zhengzhou 450052, China*
[2] *Department of Radiation Oncology, the First Affiliated Hospital of Zhengzhou University, Zhengzhou 450052, China*
[3] *Department of Colorectal Surgery, the First Affiliated Hospital of Zhengzhou University, Zhengzhou 450052, China*
[4] *Department of Clinical Laboratory, the First Affiliated Hospital of Zhengzhou University, Zhengzhou 450052, China*
[5] *Center for Clinical Laboratory, General Hospital of the Yangtze River Shipping Wuhan Brain Hospital, Wuhan 430010, China*
[6] *Henan Institute of Advanced Technology, College of Chemistry, Zhengzhou University, Zhengzhou 450001, China*
[§] *Haining Zhou and Hui Peng contributed equally to this work.*

Cite this article: *Nano Research*, **2025**, *18*, 94907292. https://doi.org/10.26599/NR.2025.94907292

ABSTRACT: Reasonable design and construction of artificial enzymes with excellent catalytic activity, good stability and superior biocompatibility is essential for tumor therapy. Single-atom site catalysts (SAs) with well-defined atomic structure and electronic coordination environments have been regarded as a new type of nanozyme that can exhibit excellent catalytic activity like natural enzymes. Here, we constructed a copper-based single-atom site nanozyme (named Cu-N,O/C) that stabilized in hollow carbon nanosphere, and the electronic structure of the single copper active center was precisely controlled by regulating the coordination of nitrogen and oxygen. The well-designed Cu-N_3O active center enables the Cu-N,O/C nanozyme to exhibit multiple extraordinary enzyme-mimicking activities by synchronously catalyzing the generation of reactive oxygen species (ROS), which can effectively inhibit the growth of tumor cell *in vitro* and *in vivo*, and the therapeutic effect pronounced enhanced in the weak acidic tumor environment. In addition, the remarkable near infrared spectroscopy (NIR)-photothermal conversion activity of Cu-N,O/C nanozyme significantly enhances the efficiency of cancer cell killing. Therefore, single-atom site nanozyme possesses significant therapeutic efficacy for tumor therapy through multiple ROS and photothermal activity.

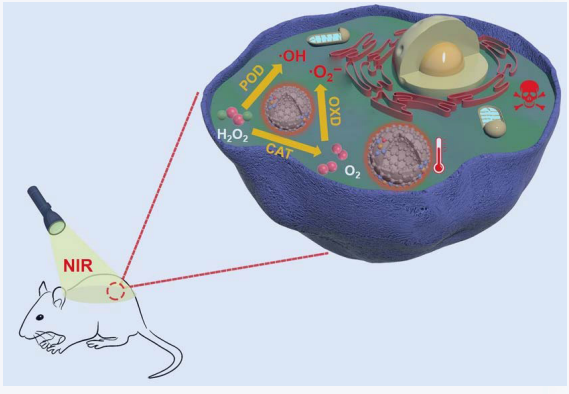

KEYWORDS: single copper atom catalysts, nanozyme, reactive oxygen species, photothermal therapy, tumor

1 Introduction

Nanomaterials with intrinsic enzyme-mimicking activities are defined as nanozymes and have been widely investigated in recent years, because of their great potential in treating numerous diseases, especially in tumor therapy [1–6]. Unlike natural enzymes that are extremely susceptible to pH, temperature, ionic strength and other environmental factors, nanozymes exhibit superior stability and recoverability in practical applications, even in complex environment and physiological conditions [7–12]. Since Fe_3O_4 nanoparticles was firstly reported to show intrinsic peroxidase-like (POD-like) activities in 2007 [4], numerous nanomaterials were subsequently discovered to exhibit highly efficient POD-like activities through generating peroxide species in biological systems, such as transition metal oxides, noble metal particles and nanocarbon materials [13–16]. Not only the POD-like activities are discovered for nanozymes, the oxidase (OXD)-like, catalase (CAT)-like and superoxide dismutase (SOD)-like activities have also been identified in recent decades [17–20]. The enzyme-mimicking activities of nanomaterials are mainly performed by catalyzing H_2O_2, O_2, or H_2O to generate the reactive oxygen species (ROS), such as superoxide anion ($\cdot O_2^-$), singlet oxygen ($^1O_2$), hydrogen peroxide (H_2O_2) and hydroxyl radical (·OH), that can damage biomolecules and induce cellular apoptosis [21–25]. Some nanozymes have been reported to exhibit not only a single ROS activity, but also the concurrent multiple ROS activities proposed to

Received: November 28, 2024; **Revised:** January 20, 2025
Accepted: February 7, 2025

✉Address correspondence to Ting Sun, sunting@zzu.edu.cn; Chang Su, changsu123456@outlook.com

significantly enhance the tumor therapeutic efficacy in practical applications [26–28]. Therefore, developing the nanozymes with highly efficient intracellular ROS activities is extremely important for tumor therapy.

In recent decades, although numerous efforts have been devoted to developing nanozymes with significantly multiple ROS activities, however, the inferior kinetics, relatively low catalytic activity, unclear active sites, and the rapid ROS elimination severely limit the further application of nanozymes. As a new type of nanozymes, single-atom site catalysts (SAs) have been regarded as the favorable alternatives to conventional enzymes in tumor therapeutics. Because of the maximum atomic utilization efficiency, unique quantum size effect, and well-defined electronic and geometric structure, single-atom site enzymes possess the highly evolved catalytic center that mimic natural enzymes at the atomic level, therefore bridging the gap between the natural enzymes and nanomaterials [29–35]. For instance, Shi and co-works reported a Cu-based SAs that can catalyze H_2O_2 and O_2 to ·OH and $\cdot O_2^-$ in the acidic tumor microenvironment without external energy consumption, the generated ROS can effectively inhibit tumor growth by oxidizing the intracellular biomolecules. Moreover, the turnover frequency (TOF) of Cu sites in nanozymes for POD-like reaction is about 5000 times larger than that of commercial Fe_3O_4 nanozyme [36]. Wu and co-works found the well-designed Mn/PSAE possess the POD-like and OXD-like activities, which were remarkably enhanced in the weak acidic tumor environment. In addition, the supported amorphous carbon exhibits an excellent photothermal conversion activity, which effectively kill tumor cells in tumor therapy applications combined with the ROS activities of Mn sites [37]. Fe-based and Ru-based SAs have also been reported to exhibit strong POD-like activities [38, 39]. Among numerous transition metals, Cu acts as the active center in some biological enzymes and can efficiently catalyze organic oxidization by oxygen [36]. Additionally, Cu exhibits versatile oxidation states and high electron transfer capacity, which are critical for mimicking enzyme activities such as POD, CAT, and OXD [36, 40, 41]. The advantage of abundant, cost-effective and interact effectively with ROS makes Cu a promising candidate for cancer therapy. Most recently reported SAs nanozymes use nitrogen-doped carbon as the substrate, in which the nitrogen atoms act as the coordination atom to anchor the metal active sites. As far as we know, the catalytic activity of SAs is mainly depended on the metal active sites and their coordination atoms. Replacing the coordinated N with lower electronegativity atoms (e.g., phosphorus and sulfur) in active center can significantly regulate the electronic structure of active center, thus effectively enhancing the catalytic activity of SAs nanozymes [42–44]. Therefore, constructing a Cu-based SAs nanozyme with expected coordination structure in active center will be more beneficial to tumor therapy.

In this work, we constructed an atomically dispersed Cu-based SAs nanozyme with Cu-N_3O active center anchored on hollow-structured carbon nanosphere, named as Cu-N,O/C nanozyme, which displays an outstanding POD-mimicking and OXD-mimicking activities by concurrently catalyzing H_2O_2 and O_2 to $\cdot O_2^-$ and ·OH through two parallel reactions, the generated ROS can efficiently induce tumor cells death through oxidization of intracellular biomolecules. The well-designed Cu-N,O/C nanozyme have been demonstrated to possess an outstanding POD-like activity and a remarkable NIR-photothermal activity. The *in vitro* and *in vivo* experiments both demonstrate that Cu-N,O/C nanozyme possesses the ability of killing cancer cell and suppressing tumor growth. This work provides a valuable reference to rational design of SAs nanozyme for tumor therapy.

2 Results and discussion

The synthesis procedure of Cu-N,O/C nanozyme is schematically illustrated in Fig. 1(a) [45]. As exhibited in Fig. 1(a), EDTA-Cu/SiO_2@PDA nanosphere with average size of about 250 nm was firstly prepared via a modified *in situ* polymerization method. Briefly, the SiO_2 nanosphere templates were gradually formed in the solution with NH_4OH and tetraethyl orthosilicate (TEOS) as raw materials, and the dopamine monomers were oxidized and polymerized *in situ* on the surface. To make the Cu active sites homogeneously distributed in the whole catalyst structure, Cu-EDTA complexes were added during synthesis. Subsequently, the obtained green EDTA-Cu/SiO_2@PDA precipitate was calcinated at 800 °C under Ar atmosphere to carbonize the polydopamine (PDA) layer, and then etched by NaOH at 70 °C to remove SiO_2 template, obtaining the hollow structured Cu single-atom site material, which is denoted as Cu-N,O/C nanozyme. The transmission electron microscopy (TEM) image in Fig. 1(b) exhibits a hollow structured nanosphere with an average size of ~ 260 nm and a wall thickness of ~ 10 nm. High resolution TEM (HRTEM) image in Fig. 1(c) displays the amorphous structure of carbon layer, and the ring-like selected area electron diffraction (SAED) pattern in Fig. 1(e) further confirms the poor crystallinity of Cu-N,O/C nanozyme. Figure 1(d) shows the atomic-resolution aberration-corrected high-angle annular dark-field scanning transmission electron microscopy (AC HAADF-STEM) image, in which homogeneous dispersed bright dots marked with red circle can be clearly observed, which are corresponding to the isolated Cu atoms anchored on the carbon framework, demonstrating the atomic dispersion of Cu atoms in Cu-N,O/C nanozyme. The energy-dispersive X-ray spectroscopy (EDS) mappings (Figs. 1(f)–1(j)) identify the uniformly distribution of C, N, O and Cu over the whole nanostructure. The content of Cu in Cu-N,O/C nanozyme is confirmed by inductively coupled plasma optical emission spectrometry (ICP-OES), and the value is 0.65 wt.%.

An only broad diffraction peak located at ~ 24° can be observed in X-ray diffraction (XRD) pattern (Fig. 1(k)) for both Cu-N,O/C and N,O/C, which is ascribed to the (002) plane of graphitic carbon, and no diffraction peaks that are corresponding to the crystalline Cu species can be observed, demonstrating the atomically dispersed Cu atoms in Cu-N,O/C nanozyme. These results are consistent with the HRTEM and AC HAADF-STEM analysis. To investigate the chemical state of the isolated Cu atoms in Cu-N,O/C nanozyme, the X-ray absorption near-edge structure (XANES) spectra of Cu-N,O/C, Cu_2O, CuO and Cu-foil were measured and the results are displayed in Fig. 1(l). As shown in Fig. 1(l), the Cu absorption edge of Cu-N,O/C is located between that of Cu_2O and CuO, indicating that the oxidation state of Cu in Cu-N,O/C is between +1 and +2. The coordination environment of Cu site in Cu-N,O/C at atomic level was further studied by extended X-ray absorption of fine structure (EXAFS), as exhibited in Fig. 1(m), only one main peak at 1.40 is found in the *R*-space EXAFS spectrum of Cu-N,O/C, which belongs to Cu–N and Cu–O bonds. Whereas no Cu–Cu characteristic peaks (2.24 Å) is detected, further demonstrating the atomically dispersed Cu sites in Cu-N,O/C nanozyme. According to the fitting results of the *R*-space EXAFS

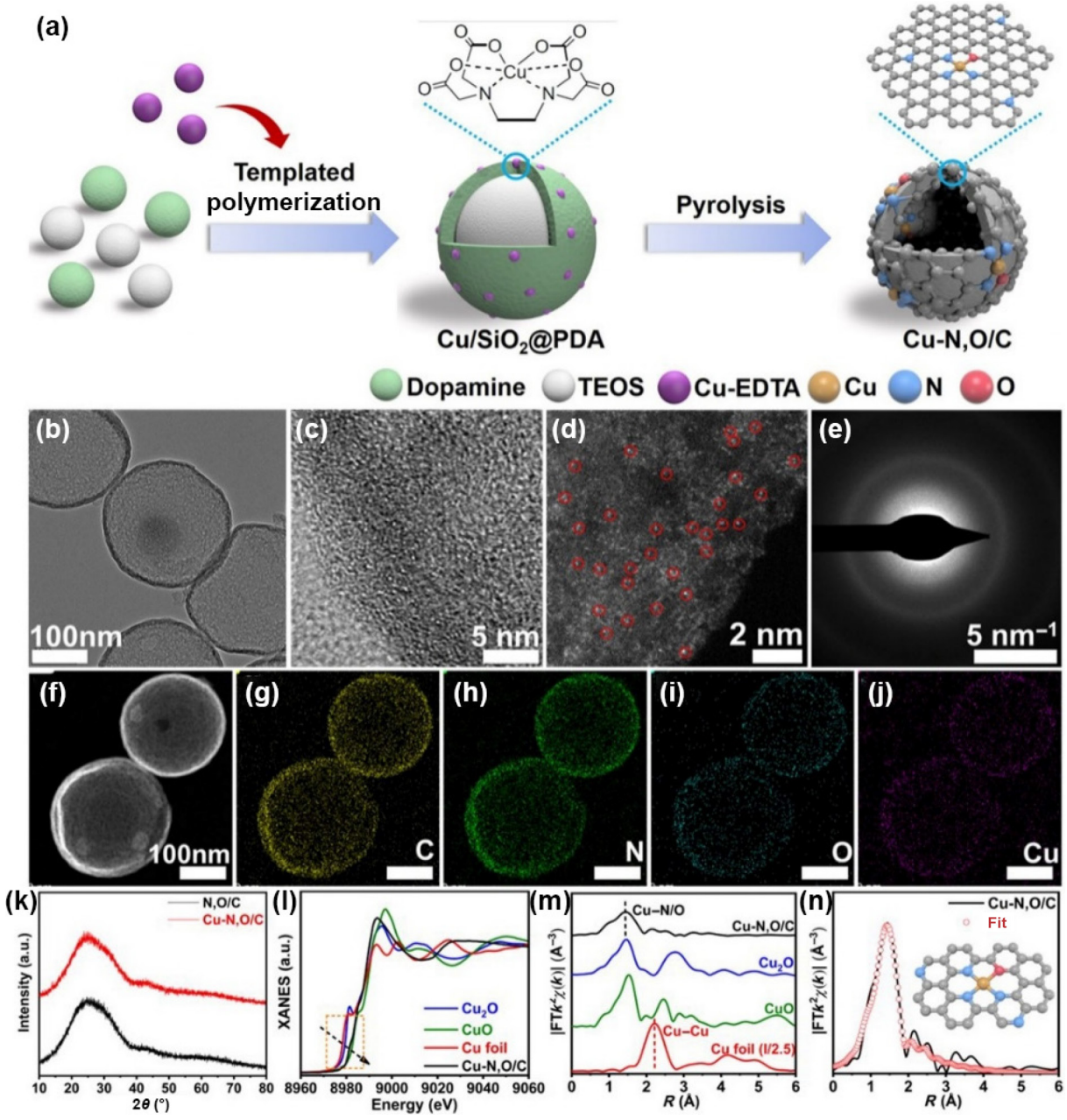

Figure 1 Preparation procedure, morphology and structural characterization of Cu-N,O/C nanozyme. (a) Schematic illustration of the formation of Cu-N,O/C nanozyme. (b) TEM, (c) HRTEM, (d) HAADF-STEM images and (e) SAED pattern of Cu-N,O/C nanozyme. (f)–(j) HAADF-STEM elemental mapping of Cu-N,O/C nanozyme. (k) XRD patterns of N,O/C and Cu-N,O/C nanozymes. (l) Cu K-edge XANES spectra of Cu-N,O/C nanozyme and reference samples. (m) Fourier transform (FT) at the Cu K-edge of Cu-N,O/C nanozyme, Cu_2O, CuO and Cu foil. (n) The measured and fitted Cu K-edge XANES spectra of Cu-N,O/C nanozyme. Inset: schematic model of Cu-N,O/C nanozyme (Cu: orange; N: blue; O: pink; C: grey).

spectrum, the proposed coordination structure of Cu center in Cu-N,O/C nanozyme is Cu-N_3O (Fig. 1(n)). The survey X-ray photoelectron spectroscopy (XPS) spectrum (Fig. S1 in the Electronic Supplementary Material (ESM)) of Cu-N,O/C nanozyme demonstrates that the chemical content of Cu-N,O/C nanozyme is Cu, N, O and C. The high-resolution C 1s XPS spectrum (Fig. S2(a) in the ESM) can be deconvoluted into graphitic sp^2 carbon (C–C, 284.8 eV), oxygen-bonded carbon (C–O, 285.3 eV, C=O, 290.2 eV), and nitrogen-bonded carbon (C–N, 286.8 eV). Figure S2(b) in the ESM exhibits the high-resolution N 1s XPS spectrum, in which five fitted peaks can be ascribed to pyridinic-N (398.5 eV), pyrrolic-N (399.4 eV), Cu coordinated N (400 eV), graphitic-N (401.1 eV), and oxidized-N (403.9 eV) [46, 47]. The high-resolution O 1s XPS spectrum is shown in Fig. S2(c) in the ESM, in which the fitted peak at 531.3 eV is ascribed to the Cu–O bond, and this is consistent with the fitting results of R-space EXAFS spectrum. Cu 2p XPS spectrum (Fig. S2(d) in the ESM) is further used to investigate the chemical valence of Cu, and the main peaks located at 932.9 and 935.1 eV are corresponding to Cu^+ and Cu^{2+}, indicating that the oxidation state of $Cu^{\delta+}$ is between 1 and 2, which agrees well with the XANES analysis.

The OXD-like and POD-like activities of Cu-N,O/C nanozyme were systematically investigated and the details are schematically illustrated in Fig. 2(a). The CAT property of Cu-N,O/C nanozyme

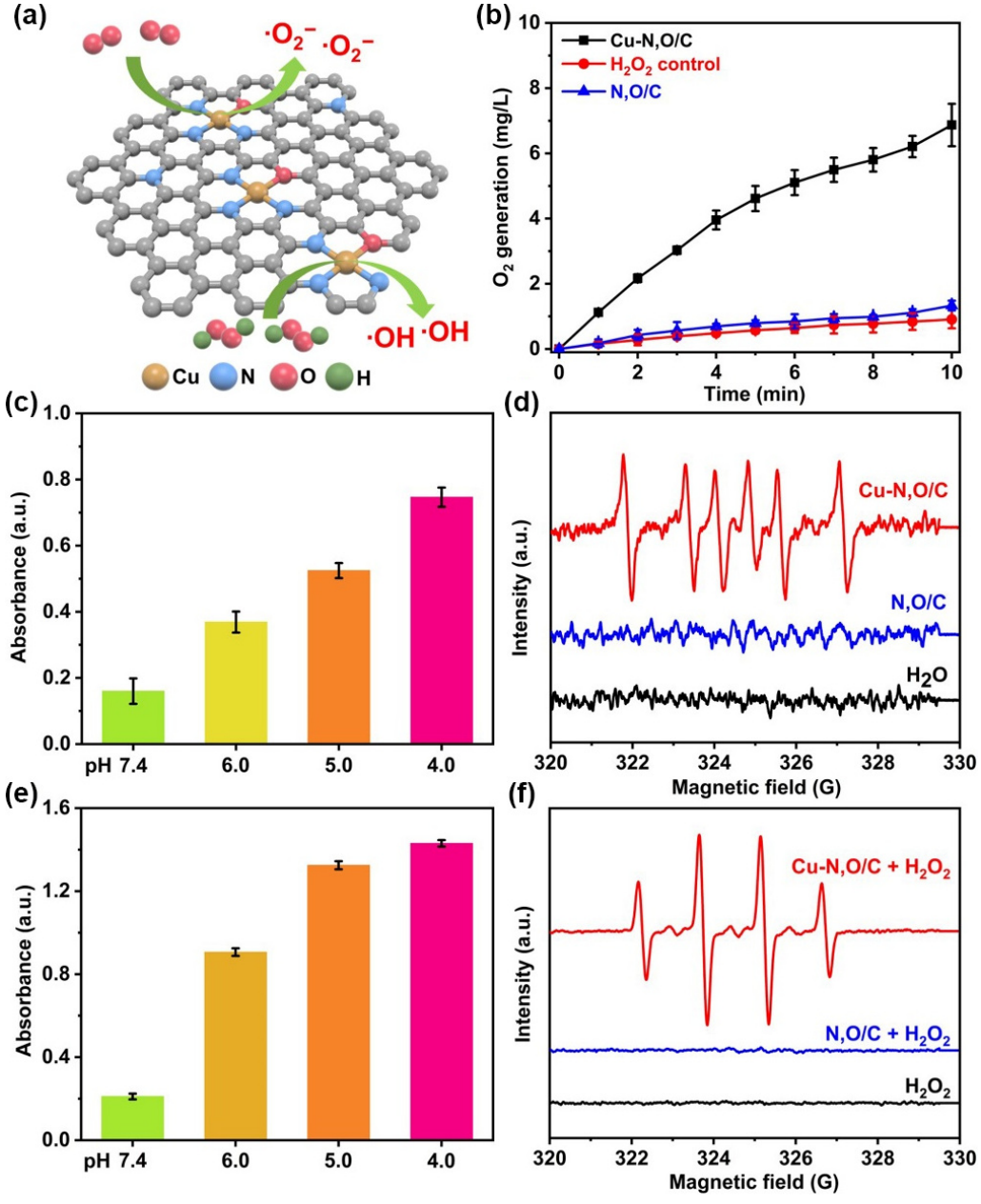

Figure 2 Catalytic performance of Cu-N,O/C nanozyme. (a) Schematic illustration of the activity of Cu-N,O/C nanozyme. (b) The O_2 generation from the decomposition of H_2O_2 by Cu-N,O/C nanozyme and N,O/C. (c) OXD-like activity of Cu-N,O/C nanozyme at different pH values. TMB: 1 mM and Cu-N,O/C nanozyme: 10 μg/mL (n = 3). (d) ESR spectra of ·OOH under different conditions. Spin adduct: BMPO. (e) POD-like activity of Cu-N,O/C nanozyme at different pH values. TMB: 1 mM, H_2O_2: 1 mM, and Cu-N,O/C nanozyme: 10 μg/mL (n = 3). (f) ESR spectra of ·OH under different conditions. Spin adduct: DMPO.

was firstly studied by catalyzing H_2O_2 to O_2. As shown in Fig. 2(b), the concentration of O_2 catalyzed by Cu-N,O/C nanozyme continuously increases as time going on, which is significantly higher than those of N,O/C and H_2O_2 control. This result confirms the excellent CAT activity of Cu-N,O/C nanozyme. To investigate the OXD-like activity of Cu-N,O/C nanozyme, the ultraviolet–visible (UV–vis) absorbance changes of 3,3',5,5'-tetramethylbenzidine (TMB) at 652 nm is monitored. The colorless TMB can be oxidized to a blue oxide, which can be quantified by detecting the UV–vis absorbance at 652 nm. As exhibited in Fig. 2(c), the marginal OXD-like activity can be observed for Cu-N,O/C nanozyme at neutral pH, and with the decrease of pH value to a weak acidic condition, the OXD-like activity of Cu-N,O/C nanozyme increases significantly. To further understand the catalytic performances of Cu-N,O/C nanozyme for the OXD-like activity, the Michaelis–Menten steady-state kinetic curve is obtained and the related parameters are calculated (Fig. S5 in the ESM), in which the V_{max} and k_m are 3.3×10^{-8} M/s and 0.1565 mM, respectively. Furthermore, to investigate the potential catalytic mechanism, electron spin resonance (ESR) is applied to monitor the possible active intermediates with 5-tertbutoxycarbonyl-5-methyl-1-pyrroline N-oxide (BMPO) as a spin trap. As shown in Fig. 2(d), an obvious characteristic BMPO/·OOH signal with intensity of 1:1:1:1:1:1 can be detected during the reaction, indicating the generation of ·OOH radicals, which identify that Cu-N,O/C nanozyme is active site for the production of $\cdot O_2^-$ radicals

during BMPO oxidation. However, no BMPO/·OOH signals are observed for N,O/C support and pure water, demonstrating that the atomically dispersed Cu atoms are the active sites for the generation of $\cdot O_2^-$ radicals. Normally, the OXD-like activity of nanozyme is based on the O_2 substrate, which can be reduced to $\cdot O_2^-$ radicals by accepting electrons. However, the O_2 content in the tumor tissues is ultralow and the H_2O_2 content is excessive. Therefore, CAT activity of Cu-N,O/C nanozyme is extremely important for the subsequently OXD-like activity, and the excellent CAT activity of Cu-N,O/C nanozyme ensures the outstanding OXD-like activity of Cu-N,O/C nanozyme.

The POD-like activity of Cu-N,O/C nanozyme is investigated by catalyzing H_2O_2 reaction, during which the H_2O_2 is catalyzed to decompose into ·OH radicals. Similar to the OXD-like activity, the generated ·OH radicals are detected by TMB, which can be oxidized by ·OH to a blue oxide and quantified by detecting the UV–vis absorbance at 652 nm. As exhibited in Fig. 2(e), Cu-N,O/C nanozyme displays a POD-like activity in a wide pH range, and the POD-like activity is enhanced when the pH value decreases, the best activity is obtained at pH 4.0. This result demonstrates that the POD-like activity of Cu-N,O/C nanozyme is acidity-dependent and more significant in tumor microenvironment. The steady-state kinetics of Cu-N,O/C nanozyme for POD-like activity are calculated based on the velocity of the TMB oxidation. The V_{max} and k_m for TMB are 17.64×10^{-8} M/s and 0.4204 mM respectively, and for H_2O_2 the V_{max} and k_m are 7.28×10^{-8} M/s and 0.3601 mM (Fig. S7 in the ESM). According to the above analysis, Cu-N,O/C nanozyme exhibits a superior POD-like activity than most of the reported nanomaterials (Table S1 in the ESM). The ESR is further used to measure the generation of ·OH radicals with 5,5-Dimethyl-1-pyrroline N-oxide (DMPO) as the spin trapper, and the result is displayed in Fig. 2(f). A characteristic quartet ESR spectra with intensity of 1:2:2:1 is obtained for Cu-N,O/C nanozyme, which is in good agreement with the characteristic spectrum of DMPO/·OH. While no DMPO/·OH characteristic peaks can be detected for N,O/C and pure H_2O_2, indicating that Cu atoms are the real active sites for catalyzing H_2O_2 to ·OH. According to the above *in vitro* analysis, the obtained Cu-N,O/C nanozyme obviously exhibits OXD-, CAT- and POD-like activities, which significantly enhanced under weak acidic conditions in the tumor microenvironment. The remarkably multiple enzymatic activities of Cu-N,O/C nanozyme indicate the potential application in cancer cell killing and tumor therapy. In addition, the durability of Cu-N,O/C nanozyme was further evaluated (Fig. S8 in the ESM), Cu atoms can retain almost 100% on the support and no Cu atoms can be detected by inductively coupled plasma mass spectrometry (ICP-MS) during 60 h incubation in both neutral and acidic conditions, indicating an excellent stability of Cu-N,O/C nanozyme.

Besides the multiple enzyme-like activities, the photothermal activity of the Cu-N,O/C nanozyme were further investigated, and the infrared thermal images are shown in Figs. S9 and S10 in the ESM. As exhibited in Figs. S9 and S10 in the ESM, the temperature of Cu-N,O/C nanozyme increases rapidly under the irradiation of 808 nm laser within 5 min, and the temperature increases obviously with increase of catalyst concentration. The maximum temperature reaches at 48.3 °C when the concentration of Cu-N,O/C nanozyme is 400 mg/mL, which is sufficient for the photothermal effect tumor elimination. Meanwhile, the photothermal stability test of Cu-N,O/C nanozyme is shown in Fig. S11 in the ESM, the photothermal activity of Cu-N,O/C nanozyme can keep stable after five cycles without any attenuation, demonstrating an excellent durability.

Next, we conducted cellular assays on Cu-N,O/C nanozyme. The intracellular ROS generation capacity was investigated by using a ROS probe 2,7-dichlorodi-hydrofluorescein diacetate (DCFH-DA). H_2O_2 is a key substrate in POD-like catalysis, and to mimic the physiological state of the tumor, 100 μM H_2O_2 was added in the cell culture for the assessment of intracellular ROS level. In confocal microscope tests, the Cu-N,O/C plus H_2O_2 group showed fluorescence intensity comparable to that of the ROS up treatment group. The group of CT-26 cells treated with Cu-N,O/C and additional H_2O_2 exhibited the strongest green fluorescence in contrast to the control and blank groups, which may be attributed to the accumulation of $\cdot O_2^-$ and ·OH radicals (Fig. S13 in the ESM). Interestingly, mild fluorescence was observed in cells treated with Cu-N,O/C alone, possibly attributed to the utilization of intracellular H_2O_2 by Cu-N,O/C nanozyme. The above results confirmed the catalytic ability of Cu-N,O/C for ROS generation in cells using H_2O_2 as substrate.

The confirmed OXD-like and POD-like activities of Cu-N,O/C nanozyme, along with its outstanding and stable photothermal conversion performance, strongly motivate further exploration of its antitumor potential. Initially, we assessed the Cu-N,O/C nanozyme-mediated inhibition of cell proliferation in CT-26 colon cancer cells. As illustrated in Fig. 3(a), at concentrations up to 200 μg/mL, Cu-N,O/C nanozyme alone showed minimal effects on cell proliferation, indicating its excellent biocompatibility. However, when cells were pre-treated with H_2O_2, the Cu-N,O/C nanozyme significantly inhibited cell proliferation in a dose-dependent manner, underscoring its pronounced antitumor effect in the presence of H_2O_2. This observation aligns with the Cu-N,O/C nanozyme's confirmed enzymatic activities. Due to its excellent photothermal conversion effect, Cu-N,O/C nanozyme also exhibited significant inhibition of cell proliferation under NIR irradiation, with a clear dose-dependent effect. Most notably, the combination of H_2O_2 and NIR irradiation with Cu-N,O/C nanozyme resulted in optimal inhibition, demonstrating a synergistic effect that maximizes tumor suppression.

The antitumor efficacy of Cu-N,O/C nanozyme on CT-26 cells can be directly observed using fluorescence imaging on cells co-stained with propidium iodide (PI) (staining dead cells in red fluorescence) and Calcein AM (staining living cells in green fluorescence). As depicted in Fig. 3(b) and Fig. S14 in the ESM, neither the solo treatments with H_2O_2, Cu-N,O/C nanozyme, nor NIR irradiation significantly affected cell viability. However, the combination of Cu-N,O/C nanozyme with H_2O_2 resulted in substantial red fluorescence, indicating marked cytotoxicity. Remarkably, in the presence of both H_2O_2 and NIR irradiation, Cu-N,O/C nanozyme led to the most prominent red fluorescence in the cells, suggesting that this treatment strategy induced the greatest cytotoxic effect. These results, consistent with the cell viability assay results, collectively indicate that the combined catalytic and photothermal effects mediated by Cu-N,O/C nanozyme can achieve synergistically enhanced antitumor effects *in vitro*. This result was further confirmed by flow cytometric measurement. As shown in Fig. 3(c), compared to catalytic killing alone, the combination of catalytic and photothermal killing mediated by Cu-N,O/C nanozyme resulted in the most significant increase in CT-26 cell apoptosis. Collectively, these results demonstrate that Cu-N,O/C nanozyme can mediate synergistic catalytic and photothermal killing, achieving enhanced antitumor effects *in vitro*.

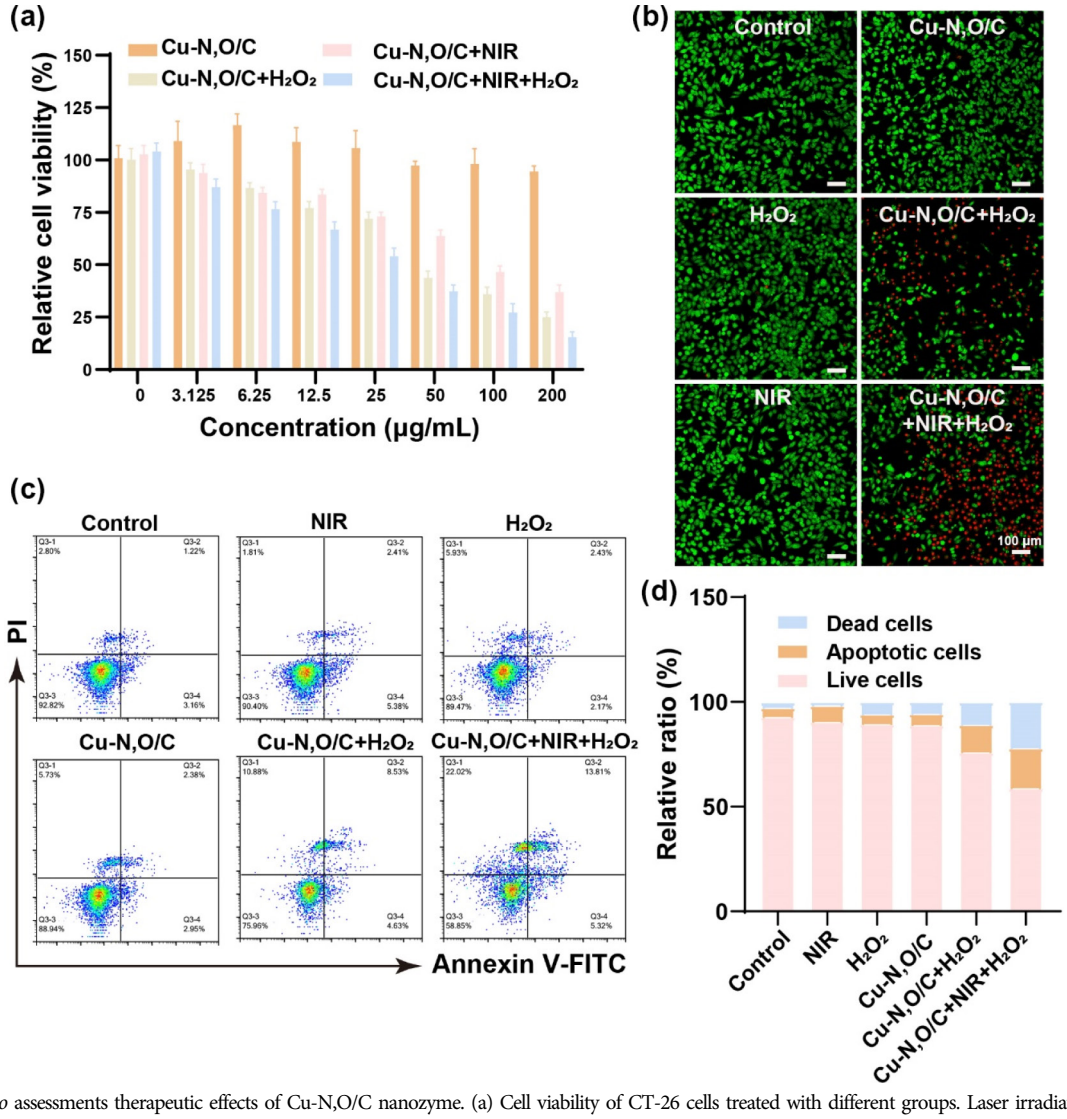

Figure 3 *In vitro* assessments therapeutic effects of Cu-N,O/C nanozyme. (a) Cell viability of CT-26 cells treated with different groups. Laser irradiation groups were irradiated under 808 nm laser for 5 min (1.0 W/cm^2). (b) Live/dead staining assay of CT-26 cells incubated with different groups. Laser irradiation groups were irradiated under 808 nm laser for 5 min (1.0 W/cm^2). Scale bars are 100 μm. (c) Flow cytometric and (d) corresponding analysis of CT-26 cells after indicated treatments. Cells were co-stained with Annexin V-FITC and PI.

Considering the biocompatible of Cu-N,O/C nanozyme *in vivo* is obscure, we initially evaluated whether Cu-N,O/C nanozyme could be injected intravenously. As shown in Fig. S15 in the ESM, the hematolysis rate of Cu-N,O/C nanozyme slightly increases at 500 μg/mL, indicating that there is no obvious toxicity of red blood cells even at 500 μg/mL. Subsequently, the half-life time of the Ce6-labeled Cu-N,O/C nanozyme during blood circulation was determined by measuring the relative fluorescence intensity in the blood of mice following intravenous injection. The calculated half-life time of the Ce6-labeled Cu-N,O/C nanozyme in mouse blood was 0.46 h (Fig. S16 in the ESM), suggesting a faster metabolic rate and higher biosafety *in vivo*. These results revealed that Cu-N,O/C nanozyme has good biocompatibility. The promising enzymatic activities and photothermal effects of Cu-N,O/C nanozyme on tumor cells encouraged us to assess its anticancer performance *in vivo*. The photothermal action of Cu-N,O/C nanozyme was evaluated on CT-26 tumor-bearing BALB/c mice. As shown in Figs. 4(a) and 4(b), *in situ* photothermal imaging showed a rapid temperature increase of 26.1 °C during the first 1 min in the Cu-N,O/C nanozyme group, and this high local temperature was maintained during the subsequent 9 min irradiation period. By comparison, only a 4 °C-temperature increase was observed in the control group treated with PBS after 10 min irradiation. The photothermal conversion efficiency (PCE) of Cu-N,O/C nanozyme was calculated to be 28.4% (Fig. S12 in the ESM).

Subsequently, we investigated the antitumor effects, leveraging both the enzymatic and photothermal properties of Cu-N,O/C nanozyme. The treatment procedure was as follows: Cu-N,O/C nanozyme was injected into tumor-bearing BALB/c mice at the dose of 15 mg/kg, followed by an 808 nm laser exposure at 1.5 W/cm^2 for 10 min. The tumor growth was monitored for 14 days post-treatment. As shown in Fig. 4(c), laser irradiation alone (group II) had no effect on tumor growth relative to the control (group I). The treatment with Cu-N,O/C nanozyme (group III) clearly inhibited tumor growth. Remarkably, the combination of Cu-N,O/C enzyme treatment and laser irradiation (group IV) significantly reduced tumor growth. After the treatment, we collected the tumors from the mice for photography and tumor

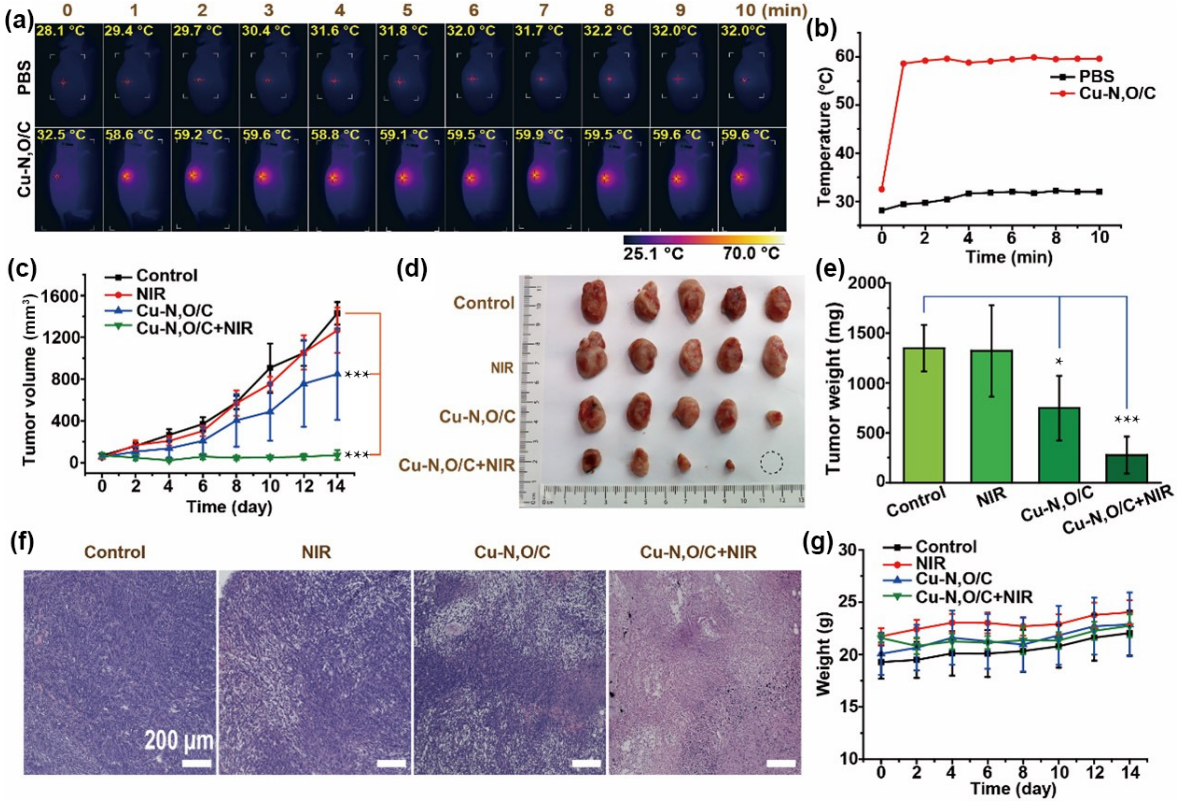

Figure 4 Photothermal-enhanced therapeutic effect of Cu-N,O/C nanozyme *in vivo*. (a) Photos of photothermal effects of Cu-N-C at different time points *in vivo*. (b) *In vivo* photothermal curves of mice at different time points. (c) Tumor growth volumes were monitored during 14 days of treatment. (d) Photo of dissected tumors after 14 days of treatment in different groups. Black dotted circles indicate complete ablation of the tumor. (e) Tumor wrights of different groups after 14 days of therapy. (f) H&E staining of tumor sections after different treatments. Scale bars are 200 μm. (g) Body-weight curves of female babl/nude mice treated with NIR or different Cu-N-C groups during 14 days of treatment (n = 5 for each group, data are shown in mean ± SD).

weight analysis. As shown in Figs. 4(d) and 4(e) and Fig. S14 in the ESM, consistent with the tumor volume monitoring data, the combination of Cu-N,O/C nanozyme treatment and laser irradiation showed the best tumor weight inhibition effect. Additionally, we performed hematoxylin and eosin (H&E) staining analysis on the collected tumor tissues. As shown in Fig. 4(f), the images of H&E staining showed severe necrosis in the Cu-N,O/C nanozyme group with NIR irradiation, in which nuclear condensation and cell shrinkage were clearly identified. Terminal deoxynucleotidyl transferase-mediated dUTP nick end labeling (TUNEL) apoptosis assay was also implemented in Fig. S17 in the ESM, it can be observed that Cu-N,O/C nanozyme + NIR induced significant apoptosis of cancer cells in tumor tissue. These results revealed the prominent anti-tumor effect of Cu-N,O/C nanozyme when combining its enzymatic activity and photothermal property.

The systemic toxicity of Cu-N,O/C nanozyme mediated therapy was evaluated by body weight measurement during the treatment. The mouse growth profiles indicated that the treatment of Cu-N,O/C nanozyme, whether with NIR irradiation or not, had no influence on the growth of mice (Fig. 4(g)). Moreover, H&E staining assay was performed on major organs and tumor tissues after the administration (Fig. S18 in the ESM). No visible damage was observed in major organs, including heart, liver, spleen, lung, and kidneys, suggesting good biocompatibility of this Cu-N,O/C nanozyme. These results indicated the high biosafety of Cu-N,O/C in potential antitumor applications. The integrated enzyme catalytic activities and PTT effects of Cu-N,O/C nanozyme significantly enhanced the anti-tumor efficiency, especially in a weak acid environment, which was comparable with those of the recently reported single-atom nanozymes and other types of metal-based nanozymes [12, 22–25, 34–41].

3 Conclusions

In summary, we designed a Cu-based single-atom site nanozyme, Cu-N,O/C, for efficient tumor therapy through combining chemical and photothermal treatment effect. Owing to the well-designed electronic structure of Cu active center, the biomimetic Cu-N,O/C nanozyme exhibits concurrent multiple OXD-like, CAT-like and POD-like activities, during which oxygen and hydrogen peroxide can be directly catalyzed into superoxide anion ($\cdot O_2^-$) and hydroxyl radical (·OH), respectively, for the oxidation and damage of target biomolecules. Moreover, the ROS activities of Cu-N,O/C nanozyme are significantly enhanced under weak acidic conditions in cancer cells, and the high level of H_2O_2 in cancer cells can also be taken advantage by Cu-N,O/C nanozyme to efficiently generate ROS for cancer cells killing. In addition, Cu-N,O/C nanozyme exhibits superior NIR-photothermal performance under 808 nm laser irradiation, and the synergistic effects of photothermal and enzyme-mimicking activities enable Cu-N,O/C nanozyme effectively kill cancer cells *in vitro* and ablation of tumors *in vivo*, confirming the excellent therapeutic effect of Cu-N,O/C nanozyme for cancer therapy. Our work provides a promising strategy for designing highly active single-atom site nanozyme with effectively multiple enzyme-mimicking and photothermal activities for tumor therapy.

Electronic Supplementary Material: Supplementary material (additional XPS results, EXAFS fitting curves, Michaelis-Menten kinetics curves, POD-like activity analysis, temperature elevation profile, near-infrared photograph, confocal microscope images, fluorescence images, and H&E staining images of major organs) is available in the online version of this article at https://doi.org/10.26599/NR.2025.94907292.

Data availability

All data needed to support the conclusions in the paper are presented in the manuscript and the Electronic Supplementary Material. Additional data related to this paper may be requested from the corresponding author upon request.

Acknowledgements

This work was supported by the Foundation for Distinguished Young Scholars of medical science and technology innovation in Henan Province (No. YXKC2022033); Fund for Scientific Research and Innovation Team of The First Affiliated Hospital of Zhengzhou University (No. QNCXTD2023018); Scientific Research Projects of colleges and universities in Henan Province (No. 24A320055).

Declaration of competing interest

All the contributing authors report no conflict of interests in this work.

Author contribution statement

C. S. and T. S.: Data curation, project administration, validation, writing manuscript, experimental design. H. N. Z.: Data curation, project administration, validation, experimental design. H. P.: Project administration, writing manuscript. Y. G. L.: Project administration, funding acquisition. T. S. and Z. Y. W.: Project administration, funding acquisition, writing manuscript. All the authors have approved the final manuscript.

Informed consent

Not applicable.

Ethics statement

The animal experiments were approved by the Animal Protection Committee of Zhengzhou University. The welfare of laboratory animals followed Laboratory animals-General code of animal welfare (GB/T 42011-2022).

Use of AI statement

None.

References

[1] Idris, N. M.; Gnanasammandhan, M. K.; Zhang, J.; Ho, P. C.; Mahendran, R.; Zhang, Y. *In vivo* photodynamic therapy using upconversion nanoparticles as remote-controlled nanotransducers. *Nat. Med.* **2012**, *18*, 1580–1585.

[2] Jiang, B.; Duan, D. M.; Gao, L. Z.; Zhou, M. J.; Fan, K. L.; Tang, Y.; Xi, J. Q.; Bi, Y. H.; Tong, Z.; Gao, G. F. et al. Standardized assays for determining the catalytic activity and kinetics of peroxidase-like nanozymes. *Nat. Protoc.* **2018**, *13*, 1506–1520.

[3] Huang, Y. Y.; Ren, J. S.; Qu, X. G. Nanozymes: Classification, catalytic mechanisms, activity regulation, and applications. *Chem. Rev.* **2019**, *119*, 4357–4412.

[4] Gao, L. Z.; Zhuang, J.; Nie, L.; Zhang, J. B.; Zhang, Y.; Gu, N.; Wang, T. H.; Feng, J.; Yang, D. L.; Perrett, S. et al. Intrinsic peroxidase-like activity of ferromagnetic nanoparticles. *Nat. Nanotechnol.* **2007**, *2*, 577–583.

[5] Liang, M. M.; Yan, X. Y. Nanozymes: From new concepts, mechanisms, and standards to applications. *Acc. Chem. Res.* **2019**, *52*, 2190–2200.

[6] Wang, Y. Q.; Huang, Y. J.; Fu, Y.; Guo, Z. X.; Chen, D.; Cao, F. X.; Ye, Q.; Duan, Q. Q.; Liu, M.; Wang, N. et al. Reductive damage induced autophagy inhibition for tumor therapy. *Nano Res.* **2023**, *16*, 5226–5236.

[7] Wu, J. J. X.; Wang, X. Y.; Wang, Q.; Lou, Z. P.; Li, S. R.; Zhu, Y. Y.; Qin, L.; Wei, H. Nanomaterials with enzyme-like characteristics (nanozymes): Next-generation artificial enzymes (II). *Chem. Soc. Rev.* **2019**, *48*, 1004–1076.

[8] Wei, H.; Wang, E. K. Nanomaterials with enzyme-like characteristics (nanozymes): Next-generation artificial enzymes. *Chem. Soc. Rev.* **2013**, *42*, 6060–6093.

[9] Wang, Z. Y.; Li, Z. Y.; Sun, Z. L.; Wang, S. R.; Ali, Z.; Zhu, S. H.; Liu, S.; Ren, Q. S.; Sheng, F. G.; Wang, B. D. et al. Visualization nanozyme based on tumor microenvironment "unlocking" for intensive combination therapy of breast cancer. *Sci. Adv.* **2020**, *6*, eabc8733.

[10] Zhu, D. M.; Ling, R. Y.; Chen, H.; Lyu, M.; Qian, H. S.; Wu, K. L.; Li, G. X.; Wang, X. W. Biomimetic copper single-atom nanozyme system for self-enhanced nanocatalytic tumor therapy. *Nano Res.* **2022**, *15*, 7320–7328.

[11] Peng, H.; Jiang, Q.; Mao, W.; Hu, Z.; Wang, Q.; Yu, Z.; Zhang, L.; Wang, X.; Zhuang, C.B.; Mai, J.; Wang, Z.Y.; Sun, T. Fe-HCOF-PEG2000 as a hypoxia-tolerant photosensitizer to trigger ferroptosis and enhance ROS-based cancer therapy. *Int. J. Nanomed.* **2024**, *19*, 1016510183.

[12] Luo, Y.; He, X. J.; Du, Q. Y.; Xu, L.; Xu, J.; Wang, J. R.; Zhang, W. L.; Zhong, Y. X.; Guo, D. J.; Liu, Y. et al. Metal-based smart nanosystems in cancer immunotherapy. *Exploration* **2024**, *4*, 20230134.

[13] Sun, H. J.; Zhou, Y.; Ren, J. S.; Qu, X. G. Carbon nanozymes: Enzymatic properties, catalytic mechanism, and applications. *Angew. Chem., Int. Ed.* **2018**, *57*, 9224–9237.

[14] Lian, M. L.; Xue, Z. J.; Qiao, X. Z.; Liu, C.; Zhang, S.; Li, X.; Huang, C. H.; Song, Q.; Yang, W. S.; Chen, X. et al. Movable hollow nanoparticles as reactive oxygen scavengers. *Chem* **2019**, *5*, 2378–2387.

[15] Liang, Y.; Liu, Y. L.; Lei, P. P.; Zhang, Z.; Zhang, H. J. Tumor microenvironment-responsive modular integrated nanocomposites for magnetically targeted and photothermal enhanced catalytic therapy. *Nano Res.* **2023**, *16*, 9826–9834.

[16] Kang, Y.; Li, C.; Shi, H. L.; Zhang, A. M.; Huang, C. S.; Zhou, C. H.; Jia, N. Q. Photothermally enhanced dual enzyme-mimic activity of gold-palladium hybrid nanozyme for cancer therapy. *Chin. J. Chem.* **2023**, *41*, 3189–3196.

[17] Chen, D.; Xia, Z. M.; Guo, Z. X.; Gou, W. Y.; Zhao, J. L.; Zhou, X. M.; Tan, X. H.; Li, W. B.; Zhao, S. J.; Tian, Z. M. et al. Bioinspired porous three-coordinated single-atom Fe nanozyme with oxidase-like activity for tumor visual identification via glutathione. *Nat. Commun.* **2023**, *14*, 7127.

[18] Wang, X. Z.; Ren, X. F.; Yang, J.; Zhao, Z. C.; Zhang, X. Y.; Yang, F.; Zhang, Z. Y.; Chen, P.; Li, L. P.; Zhang, R. P. Mn-single-atom nano-multizyme enabled NIR-II photoacoustically monitored, photothermally enhanced ROS storm for combined cancer therapy. *Biomater. Res.* **2023**, *27*, 125.

[19] Wang, X. Y.; Chen, Q.; Zhu, Y. F.; Wang, K. R.; Chang, Y. L.; Wu, X. W.; Bao, W. C.; Cao, T. C.; Chen, H. R.; Zhang, Y. et al.

Destroying pathogen-tumor symbionts synergizing with catalytic therapy of colorectal cancer by biomimetic protein-supported single-atom nanozyme. *Signal Transduct. Target. Ther.* **2023**, *8*, 277.
[20] Wei, G.; Liu, S. J.; Peng, Y. K.; Wei, H. On the specificity of nanozymes: A perspective. *Chin. J. Chem.* **2024**, *42*, 1515–1522.
[21] Ren, G. Y.; Lu, M. J.; Zhao, Z. Q.; Qin, F. J.; Li, K.; Chen, W. X.; Lin, Y. Q. Cobalt single-atom nanozyme Co-administration with ascorbic acid enables redox imbalance for tumor catalytic ablation. *ACS Biomater. Sci. Eng.* **2023**, *9*, 1066–1076.
[22] Wang, X. W.; Shi, Q. Q.; Zha, Z. B.; Zhu, D. D.; Zheng, L. R.; Shi, L. X.; Wei, X. W.; Lian, L.; Wu, K. L.; Cheng, L. Copper single-atom catalysts with photothermal performance and enhanced nanozyme activity for bacteria-infected wound therapy. *Bioact. Mater.* **2021**, *6*, 4389–4401.
[23] Wang, M.; Yang, C. Z.; Chang, M. Y.; Xie, Y. L.; Zhu, G. Q.; Qian, Y. R.; Zheng, P.; Sun, Q. Q.; Lin, J.; Li, C. X. Single-atom nanozymes based nanobee vehicle for autophagy inhibition-enhanced synergistic cancer therapy. *Nano Today* **2023**, *52*, 101981.
[24] Peng, C.; Pang, R. Y.; Li, J.; Wang, E. R. Current advances on the single-atom nanozyme and its bioapplications. *Adv. Mater.* **2024**, *36*, 2211724.
[25] Zhang, G. Q.; Wang, N.; Ma, Y.; Zhai, S. M.; Ngai, T.; Ni, S. L.; Jiang, X. Y.; Jiao, J. W.; Cui, J. W. Metal coordination-driven assembly of stimulator of interferon genes-activating nanoparticles for tumor chemo-immunotherapy. *BMEMat* **2024**, *2*, e12077.
[26] Wang, Z. H.; Wu, F. G. Emerging single-atom catalysts/nanozymes for catalytic biomedical applications. *Adv. Healthc. Mater.* **2022**, *11*, 2101682.
[27] He, W. Y.; Wu, J. H.; Liu, J. L.; Li, J. Single-atom nanozymes for catalytic therapy: Recent advances and challenges. *Adv. Funct. Mater.* **2024**, *34*, 2312116.
[28] Xing, Y. X.; Wang, L.; Wang, L. C.; Huang, J. X.; Wang, S.; Xie, X. Y.; Zhu, J.; Ding, T.; Cai, K. Y.; Zhang, J. X. Flower-like nanozymes with large accessibility of single atom catalysis sites for ROS generation boosted tumor therapy. *Adv. Funct. Mater.* **2022**, *32*, 2111171.
[29] Jiang, B.; Guo, Z. J.; Liang, M. M. Recent progress in single-atom nanozymes research. *Nano Res.* **2023**, *16*, 1878–1889.
[30] Cai, S. F.; Zhang, W.; Yang, R. Emerging single-atom nanozymes for catalytic biomedical uses. *Nano Res.* **2023**, *16*, 13056–13076.
[31] Tao, N.; Chen, S. H.; Mahdinloo, S.; Zhang, Q. Y.; Lan, T. F.; Saiding, Q.; Chen, S. Y.; Xiong, Y.; Tao, W.; Ouyang, J. A pH-responsive single-atom nanozyme for photothermal-augmented nanocatalytic tumor therapy. *Nano Today* **2024**, *57*, 102371.
[32] Shen, J.; Chen, J.; Qian, Y. P.; Wang, X. Q.; Wang, D. S.; Pan, H. G.; Wang, Y. G. Atomic engineering of single-atom nanozymes for biomedical applications. *Adv. Mater.* **2024**, *36*, 2313406.
[33] Chen, Y. J.; Jiang, B.; Hao, H. G.; Li, H. J.; Qiu, C. Y.; Liang, X.; Qu, Q. Y.; Zhang, Z. D.; Gao, R.; Duan, D. M. et al. Atomic-level regulation of cobalt single-atom nanozymes: Engineering high-efficiency catalase mimics. *Angew. Chem., Int. Ed.* **2023**, *62*, e202301879.
[34] Jiang, P.; Zhang, L. D.; Liu, X. L.; Ye, C. L.; Zhu, P.; Tan, T.; Wang, D. S.; Wang, Y. G. Tuning oxidant and antioxidant activities of ceria by anchoring copper single-site for antibacterial application. *Nat. Commun.* **2024**, *15*, 1010.
[35] Ou, H. H.; Qian, Y. P.; Yuan, L. T.; Li, H.; Zhang, L. D.; Chen, S. H.; Zhou, M.; Yang, G. D.; Wang, D. S.; Wang, Y. G. Spatial position regulation of Cu single atom site realizes efficient nanozyme photocatalytic bactericidal activity. *Adv. Mater.* **2023**, *35*, 2305077.
[36] Lu, X. Y.; Gao, S. S.; Lin, H.; Yu, L. D.; Han, Y. H.; Zhu, P. A.; Bao, W. C.; Yao, H. L.; Chen, Y.; Shi, J. L. Bioinspired copper single-atom catalysts for tumor parallel catalytic therapy. *Adv. Mater.* **2020**, *32*, 2002246.
[37] Zhu, Y.; Wang, W. Y.; Cheng, J. J.; Qu, Y. T.; Dai, Y.; Liu, M. M.; Yu, J. N.; Wang, C. M.; Wang, H. J.; Wang, S. C. et al. Stimuli-responsive manganese single-atom nanozyme for tumor therapy via integrated cascade reactions. *Angew. Chem., Int. Ed.* **2021**, *60*, 9480–9488.
[38] Yang, Q. Y.; Liu, J. W.; Cai, W. T.; Liang, X.; Zhuang, Z. C.; Liao, T.; Zhang, F. X.; Hu, W. K.; Liu, P. X.; Fan, S. J. et al. Non-heme iron single-atom nanozymes as peroxidase mimics for tumor catalytic therapy. *Nano Lett.* **2023**, *23*, 8585–8592.
[39] Wang, W. Y.; Zhu, Y.; Zhu, X. R.; Zhao, Y. F.; Xue, Z. G.; Xiong, C.; Wang, Z. Y.; Qu, Y. T.; Cheng, J. J.; Chen, M. et al. Biocompatible ruthenium single-atom catalyst for cascade enzyme-mimicking therapy. *ACS Appl. Mater. Interfaces* **2021**, *13*, 45269–45278.
[40] Bai, J. X.; Feng, Y. H.; Li, W. M.; Cheng, Z. R.; Rosenholm, J. M.; Yang, H. L.; Pan, G. Q.; Zhang, H. B.; Geng, D. C. Alternative copper-based single-atom nanozyme with superior multienzyme activities and NIR-II responsiveness to fight against deep tissue infections. *Research* **2023**, *6*, 0031.
[41] Zhong, S. J.; Xiong, C.; Zhao, Y. C.; Yao, S. C.; Hu, Q. H.; Wang, S. B.; Zhao, Q. Y.; Li, L. L. Self-driven electricity modulates d-band electrons of copper single-atom nanozyme for boosting cancer therapy. *Adv. Funct. Mater.* **2023**, *33*, 2305625.
[42] Lin, L. H.; Li, H.; Gu, H. F.; Sun, Z. Y.; Huang, J.; Qian, Z. N.; Li, H.; Liu, J. Z.; Xi, H. Y.; Wu, P. F. et al. Asymmetrically coordinated single-atom iron nanozymes with Fe–N_1C_2 structure: A peroxidase mimetic for melatonin detection. *Nano Res.* **2023**, *16*, 4751–4757.
[43] Ji, S. F.; Jiang, B.; Hao, H. G.; Chen, Y. J.; Dong, J. C.; Mao, Y.; Zhang, Z. D.; Gao, R.; Chen, W. X.; Zhang, R. F. et al. Matching the kinetics of natural enzymes with a single-atom iron nanozyme. *Nat. Catal.* **2021**, *4*, 407–417.
[44] Chan, M. H.; Chen, B. G.; Huang, W. T.; Su, T. Y.; Hsiao, M.; Liu, R. S. Tunable single-atom nanozyme catalytic system for biological applications of therapy and diagnosis. *Mater. Today Adv.* **2023**, *17*, 100342.
[45] Xiong, W. F.; Li, H. F.; Wang, H. M.; Yi, J. D.; You, H. H.; Zhang, S. Y.; Hou, Y.; Cao, M. N.; Zhang, T.; Cao, R. Hollow mesoporous carbon sphere loaded Ni–N_4 single-atom: Support structure study for CO_2 electrocatalytic reduction catalyst. *Small* **2020**, *16*, 2003943.
[46] Xu, B. L.; Li, S. S.; Zheng, L. R.; Liu, Y. H.; Han, A. L.; Zhang, J.; Huang, Z. J.; Xie, H. J.; Fan, K. L.; Gao, L. Z. et al. A bioinspired five-coordinated single-atom iron nanozyme for tumor catalytic therapy. *Adv. Mater.* **2022**, *34*, 2107088.
[47] Lv, Q. Y.; Chi, K.; Shi, X. L.; Liu, M. D.; Li, X. Y.; Zhou, C.; Shi, L.; Fan, H. L.; Liu, H.; Liu, J. et al. Nanozyme-like single-atom catalyst combined with artesunate achieves photothermal-enhanced nanocatalytic therapy in the near-infrared biowindow. *Acta Biomater.* **2023**, *158*, 686–697.